

Abstract

This paper presents the reconstruction of the 73 year time series of the aerosol optical depth (AOD) at 500 nm at the subtropical high-mountain Izaña Atmospheric Observatory (IZO) located in Tenerife (Canary Islands, Spain). For this purpose, we have combined AOD estimates from artificial neural networks (ANNs) from 1941 to 2001 and AOD measurements directly obtained with a Precision Filter Radiometer (PFR) between 2003 and 2013. The analysis is limited to summer months (July–August–September), when the largest aerosol load is observed at IZO (Saharan mineral dust particles). The ANN AOD time series has been comprehensively validated against co-incident AOD measurements performed with a solar spectrometer Mark-I (1984–2009) and AERONET (AERosol ROBotic NETwork) CIMEL photometers (2004–2009) at IZO, obtaining a rather good agreement on a daily basis: Pearson coefficient, R , of 0.97 between AERONET and ANN AOD, and 0.93 between Mark-I and ANN AOD estimates. In addition, we have analyzed the long-term consistency between ANN AOD time series and long-term meteorological records identifying Saharan mineral dust events at IZO (synoptical observations and local wind records). Both analyses provide consistent results, with correlations larger than 85 %. Therefore, we can conclude the reconstructed AOD time series captures well the AOD variations and dust-laden Saharan air mass outbreaks at short-term and long-term time scales and, thus, it is suitable to be used in climate analysis.

1 Introduction

Solar radiation reaching the Earth's surface (SSR) plays a key role in our climate and environment. In the last decades, numerous analyses have demonstrated that SSR records have not been constant over time, but have undergone climatologically significant decadal variations (e.g. Pallé and Butler, 2001; Stanhill and Cohen, 2001; Sanchez-Lorenzo et al., 2007; Wild, 2009; García et al., 2014a). From the 1930s to

AMTD

8, 9075–9103, 2015

1941–2013 AOD time series at IZO from ANNs

R. D. García et al.

Title Page

Abstract

Introduction

Conclusions

References

Tables

Figures



Back

Close

Full Screen / Esc

Printer-friendly Version

Interactive Discussion



1941–2013 AOD time series at IZO from ANNs

R. D. García et al.

Title Page

Abstract

Introduction

Conclusions

References

Tables

Figures



Back

Close

Full Screen / Esc

Printer-friendly Version

Interactive Discussion



the early 1950s the few data available suggest an increase of the SSR in the first part of the 20th century, known as early brightening. This period is followed by a widespread period of reduced solar radiation from the 1950s to the end of the 1990s. This effect, extensively reported by the literature at a global scale, is known as dimming, with a general decline between 4 and 6% decade⁻¹ considering worldwide distributed stations. Recently, a gradual increase of the SSR has been documented, known as brightening, with trends between +1 and +11% decade⁻¹ from the 1980s onwards (Ohmura and Lang, 1989; De Bruin et al., 1995; Gilgen et al., 1998; Stanhill and Cohen, 2001; Ohmura, 2006; Wild et al., 2005; Sanchez-Lorenzo et al., 2007; Wild et al., 2008; Wild, 2009; García et al., 2014a).

The causes of these phenomena are not fully understood currently, but it has been pointed as most probably the changes in the transmissivity of the Earth's atmosphere. These changes might be due to changes on global cloud cover and atmospheric aerosol concentrations. Wild et al. (2005) found that the changes are observed under all cloud-cover conditions, thus probably the most important cause is the aerosol effects (Kaufman et al., 2002). In this context, the study of the spatial and temporal variability of atmospheric aerosols at sites in background conditions can offer crucial insights to account for their key role on the observed SSR trends. For this purpose, reliable long-term series of aerosol content and properties are fundamental. However, these long-term series are only available typically since the middle of the 1970s, due to the poor data quality and changes in measurements methodology before this date. There are few studies treating aerosol long-term series in the literature. The longest available series are those of normal direct irradiance measured at various stations in Russia, Ukraine and Estonia covering together a 102 year period (1906–2007) with which the atmospheric transparency has been estimated (Ohvriil et al., 2009). Kudo et al. (2011) estimated aerosol optical depth (AOD) combining broadband direct and diffuse irradiance measurements performed at Tsukuba, Japan, from 1975 to 2008. Shaw (1979) and Holben et al. (2001) studied long-term series of AOD from sun photometry at Mauna Loa since 1976, and Barreto et al. (2014) derived AOD from solar

irradiance measurements at Izaña Atmospheric Observatory (IZO) since 1976. All of these studies are based on solar spectrometry, but a different approach is needed to obtain longer AOD time series.

One of the most powerful tools used in science in the last decades are the artificial neural networks (ANNs). The ANNs have been employed in diverse applications and fields such as robotics, pattern recognition, forecasting, medicine, power systems, etc. In atmospheric science the use of ANNs is quite recent, for example, ANNs have been successfully used for estimating solar radiation values (Mohandes et al., 1998; Dorvlo et al., 2002; López et al., 2005; Feister and Junk, 2006; Junk et al., 2007; Feister et al., 2008; Paoli et al., 2009; Linares-Rodríguez et al., 2011, 2013) or cloud properties (González et al., 2002; Cerdeña et al., 2006). However, its use for AOD estimations is quite recent and limited to short periods. For example, Cazorla et al. (2008) estimated AOD values from All-Sky images at Granada (Spain) between 2005 and 2006, finding uncertainties of 0.019 and 0.014 for AOD at 440 and 670 nm, respectively, by comparing with AERONET (AERosol RObotic NETwork; <http://aeronet.gsfc.nasa.gov>) AOD observations. Also, Foyo-Moreno et al. (2014) used ANNs to obtained AOD from global, diffuse and direct normal irradiance in Granada between 2006 and 2008. They found uncertainties of $\sim 13\%$ respect to AERONET AOD values.

In this context, the goal of this paper is to estimate the long-term AOD time series of Saharan mineral dust events at IZO and to document its quality and long-term consistency by a comprehensive validation study. This has been done by using ANN techniques and, as input parameters, in-situ meteorological observations performed at IZO between 1941 and 2001. The estimated ANN AOD time series has been completed with AOD observations from sunphotometry since 2003. Given the strategic location of IZO, very close to the Saharan desert, the reconstructed ANN AOD time series provide interesting clues on the intensity and the interannual and interdecadal variability of Saharan dust outbreaks over the North Atlantic. This might have important implications for climate analysis. To address this study, this paper has been divided in five sections. Section 2 describes the main characteristics of the site where the ANN AOD estimates

1941–2013 AOD time series at IZO from ANNs

R. D. García et al.

[Title Page](#)[Abstract](#)[Introduction](#)[Conclusions](#)[References](#)[Tables](#)[Figures](#)[Back](#)[Close](#)[Full Screen / Esc](#)[Printer-friendly Version](#)[Interactive Discussion](#)

have been obtained (IZO), while Sect. 3 presents the architecture, training process and input parameters used to select the optimal ANN configuration, as well as an error analysis of ANN AOD estimations. Section 4 shows the validation of ANN AOD estimates with coincident AOD measurements, whereas the comparison between long-term ANN AOD and meteorological records is addressed in Sect. 5. Finally, a summary and the main conclusions are given in Sect. 6.

2 Description of site and aerosol conditions

Izaña Atmospheric Observatory (<http://izana.aemet.es>) is a high-mountain observatory located in Tenerife (Canary Islands) at 28.3° N, 16.5° W, 2373 m.a.s.l., and situated approximately 300 km west from the African coast (Fig. 1a). IZO is managed by the Izaña Atmospheric Research Center (IARC) which forms part of the Meteorological State Agency of Spain (AEMET).

The observatory is located above a strong subtropical temperature inversion layer, which acts as a natural barrier for local pollution (Fig. 1b). In addition, IZO is affected by a quasi-permanent subsidence regime typical of subtropical latitudes, therefore the air surrounding the observatory is representative of the background free troposphere (especially at night-time). The combination of these two features makes IZO excellent for in-situ and remote sensing atmospheric measurements and explains the history of the observatory. The first meteorological observations date from 1916 (DGIGE, 1915). In 1984 IZO became a World Meteorological Organization (WMO) Background Atmospheric Pollution Monitoring Network (BAPMon), and afterwards (1989), a Global Atmosphere Watch (GAW) station. Currently, there is a comprehensive measurement programme to monitor the atmospheric composition. IZO has been part of NDACC (Network for the Detection of Atmospheric Composition Change) since 2001, and has actively contributed to international aerosols and radiation networks such as GAW/PFR (Precision Filter Radiometer Network) since 2001, AERONET (Aerosol Robotic Network) since 2004 and BSRN (Baseline Surface Radiation Network) since 2009. In

Title Page

Abstract

Introduction

Conclusions

References

Tables

Figures



Back

Close

Full Screen / Esc

Printer-friendly Version

Interactive Discussion



Eastern North Atlantic. Note that, hereafter, we use AOD medians instead of means because the AOD values dramatically change orders of magnitude from background conditions to dusty conditions. The errors are given as $\pm 1\text{SEM}$ (standard error of the median).

3 Artificial neural networks (ANNs)

ANNs are statistical data modeling tools, inspired by the human brain, capable of simulating highly non-linear and complex relationships between inputs and outputs by a learning process. This tool mainly consists in three layers of neurons: the input layer groups the input data and connects them with the hidden layer, where the layer of neurons processes the input information with the adaptive weights obtained in the learning procedure. Finally, the hidden layer is connected with the output layer, in which the transfer function processes the input data to obtain the outputs or targets (Jain et al., 1996, and references therein).

In this work, the ANNs have been implemented by using the Matlab Neural Network Toolbox (Demuth and Beale, 1993) with the architecture shown in Fig. 3: an input layer with different meteorological observations taken at IZO as input parameters (Sect. 3.2 details the selection of these inputs), a hidden layer made up of 30 neurons, and a transfer function φ defined by the hyperbolic tangent function (Eq. 1). Our target parameter is AOD at 500 nm (hereafter ANN AOD).

$$\varphi = \tanh(\chi) = \frac{e^{2\chi} - 1}{e^{2\chi} + 1} \quad (1)$$

where χ is the corresponding input.

3.1 Training process

The learning or training procedure plays a key role in the ANNs design and setting. In this process a set of inputs with their known outputs are used to evaluate the accuracy

1941–2013 AOD time series at IZO from ANNs

R. D. García et al.

Title Page

Abstract

Introduction

Conclusions

References

Tables

Figures



Back

Close

Full Screen / Esc

Printer-friendly Version

Interactive Discussion



1941–2013 AOD time series at IZO from ANNs

R. D. García et al.

Title Page

Abstract

Introduction

Conclusions

References

Tables

Figures



Back

Close

Full Screen / Esc

Printer-friendly Version

Interactive Discussion



on the variability of the VIS, we only work with cloud-free days filtered with an average sky cover of 0 oktas. Furthermore, we have introduced the fraction clear sky (FCS) defined as the ratio between the maximum daily sunshine duration SD_{max} and SD performed with Campbell-Stokes sunshine recorder (García et al., 2014a) to account for the remaining variability introduced by the presence of clouds, fog, etc. To complete the characterization of the meteorological conditions, we have considered the relative humidity (RH) and temperature records (T). The latter inputs are only available every 3 h between 06:00 and 18:00 UTC, thereby we have calculated the daily medians. Finally, to account for the seasonal variation of each parameter we have also introduced the day of year (Nd) as input parameter. The time series at IZO range from 1916 and 1921 to present for T/RH and FCS, respectively, and from 1941 to 2009 for VIS. Therefore, the latter time series determines the period in which the ANN AOD time series can be estimated with ANN techniques: 1941–2009. These data were taken from the AEMET climatological database (<http://www.aemet.es>).

In order to study the relative importance of each input parameter and select the best configuration, several combinations of the input parameters has been trained, validated and tested in the period 2003–2009 (period with coincident PFR AOD and input parameter measurements). The different combinations considered were: (A) Nd and VIS; (B) Nd, VIS and FCS; (C) Nd, VIS, FCS and RH; and (D) Nd, VIS, FCS, RH and Temp. As observed in Table 1, the VIS and FCS are the most critical parameters determining $\sim 90\%$ of the observed AOD variance, although the maximum agreement is achieved when the RH is also taken into account as input parameter (setup C). This configuration accounts for 98 % of the actual AOD variability with a slope of 0.99 and intercept of -0.01 between the measured and estimated AOD values. By applying this setup, we have obtained the daily ANN AOD time series between 1941 and 2009 at IZO, which is displayed in Fig. 4 on a monthly basis.

To analyze how the ANN AOD estimates could be affected by uncertainties in the input parameters used, we have performed a two-step theoretical error estimation based on: first, AOD estimations were conducted using the measured values for all param-

1941–2013 AOD time series at IZO from ANNs

R. D. García et al.

[Title Page](#)[Abstract](#)[Introduction](#)[Conclusions](#)[References](#)[Tables](#)[Figures](#)[Back](#)[Close](#)[Full Screen / Esc](#)[Printer-friendly Version](#)[Interactive Discussion](#)

eters described in the previous section, obtaining the non-perturbed values (AOD). In a second step, we have simulated again the same sample by applying the typical uncertainties of the inputs parameters reported in the literature, $\pm 5\%$ for FCS (García et al., 2014a) and $\pm 2\%$ for RH (Thies, 2011). For the horizontal visibility we have assumed a very conservative error of $\pm 25\%$. Note that the day of year has been omitted from this analysis.

This strategy was applied to all cloud-free days (oktas = 0) between 2003 and 2009 in order to detect random and systematic behaviours in the error time series (AOD $\pm \delta$) (García et al., 2014b). As the theoretical error distributions have not shown dependence either on the input parameters or on the ANN AOD values (correlation is not significant at 95 % level of confidence), the systematic and random errors have been calculated as the median and the standard deviation of the corresponding error distributions.

The results of our error analysis are summarized in Table 2, where the two prevalent atmospheric situations observed at IZO have been distinguished: free-troposphere background conditions with AOD ≤ 0.10 and $\alpha \geq 0.75$, and Saharan dust events with AOD ≥ 0.20 and $\alpha \leq 0.50$. As expected, the uncertainties of the FCS and VIS dominate the random and systematic error budgets for all the AOD ranges. For AOD ≤ 0.10 the scatter reaches 0.12 and the systematic error is -0.02 , while for AOD ≥ 0.20 we obtain a scatter of 0.17, and a bias of 0.03. When considering all the AOD range and all the input parameter errors, the overall uncertainty is expected to be less than 0.15 (SD), with a positive bias of 0.03.

4 Validation of ANN AOD estimates

The ANN AOD estimates have been validated with coincident AERONET CIMEL photometers Level 2.0 AOD (cloud screened and quality ensured) from 2004 to 2009, and with a long-term AOD at 769.9 nm data series retrieved by Barreto et al. (2014) from a solar spectrometer Mark-I for the period 1975–2012.

1941–2013 AOD time series at IZO from ANNs

R. D. García et al.

Title Page

Abstract

Introduction

Conclusions

References

Tables

Figures



Back

Close

Full Screen / Esc

Printer-friendly Version

Interactive Discussion



CIMEL photometers retrieves AOD measurements at different wavelengths between 340–1640 nm from direct Sun observations under cloud-free conditions, with an expected uncertainty of 0.01 at 500 nm for field instruments (Eck et al., 1999). The validation procedure of Mark-I AOD time series was performed by Barreto et al. (2014), showing a root-mean-square error of 0.022 ($R = 0.94$) and 0.034 ($R = 0.92$) in comparison with the PFR reference and AERONET master instruments, respectively. In order to compare the Mark-I AOD values at 769.9 nm and the ANN AOD estimates at 500 nm, we have extrapolated the ANN AOD values from 500 to 769.9 nm by using the Angström's Law (Angstrom, 1929) and the α data retrieved from PFR observations. From Mark-I we have used the AOD records since 1984 when the observations start to be seamlessly performed.

The straightforward comparisons between AOD observations and estimates show a good agreement for the daily values with $\sim 94\%$ ($R = 0.97$) of the variance in agreement between AERONET AOD and ANN AOD, and 85% ($R = 0.93$) between Mark-I AOD and ANN AOD values (Fig. 5a and b). When considering monthly values the agreement increases, achieving a correlation of 96 and 98% with Mark-I/ANN and AERONET/ANN, respectively. Although the comparison with the Mark-I AOD records shows a poorer agreement, both inter-comparisons behave similarly. We observe that the ANN AOD estimates have shown to be dependent on the AOD range (see Table 3), confirming the results obtained in the theoretical error estimation (Table 2). For low AOD, the ANN AOD values tend to overestimate compared with the observed AOD values (median bias of ~ 0.01 – 0.02), but the contrary behavior is observed for high AOD (underestimation by 0.01 – 0.03). However, the overall ANN AOD/ Mark-I AOD scatter (0.06) duplicates the observed for the ANN AOD/AERONET AOD comparison (0.03). This agreement is within the AOD uncertainty of Mark-I (Barreto et al., 2014) and within our error estimation (Table 2). Notice that the experimental scatter is significantly smaller than the theoretical one, suggesting that our assumed uncertainties could be very conservative. Therefore, in summary, we consider that the ANN AOD

(Fig. 6c). Therefore, we have analyzed the relation between the monthly AOD medians in July (month with the maximum frequency of Saharan dust events at IZO in the study period) and the monthly percentage of time the wind is blowing from each of the four quadrants for the period 1941–2009. Both analyses provide consistent results. On one hand, we found that the number of days with 05–06 Synop codes time series agrees with the number of days with ANN AOD ≥ 0.20 time series ($R = 0.89$). On the other hand, a high correlation ($R = 0.86$) between the ANN AOD monthly medians and the percentage of time the wind blows in the second quadrant is observed, whilst no correlation at all is found in the other three quadrants (R of 0.24, 0.16 and 0.14, for the first, third and fourth quadrants, respectively) (see Fig. 6c and d). These results show that the reconstructed ANN AOD series correlate well with other series of independent atmospheric parameters, confirming its consistency in this long period (1941–2009), and probing its capability for tracking inter-annual variations of dust-laden Saharan air mass outbreaks. The ANN AOD series is suitable to be used in climate analysis.

6 Summary and conclusions

This paper presents, for the first time, the AOD time series of Saharan mineral dust outbreaks over the subtropical North Atlantic between 1941 and 2013. This has been done at the Izaña Atmospheric Observatory (IZO), frequently affected by the Saharan Air layer during the summer months, and by combining AOD estimates from artificial neural networks (ANNs) between 1941 and 2001, and AOD measurements during the period 2003–2013.

The ANNs method has proved to be a very useful tool for the reconstruction of daily AOD values at 500 nm from meteorological input data, such as the horizontal visibility, fraction of clear sky, and relative humidity, recorded at IZO. ANN AOD estimates adequately captures the day-to-day AOD variations and the long-term trends as compared to coincident AOD measurements from Mark-I solar spectrometer (1984–2009) and AERONET (2004–2009). The results show a good agreement for the daily

1941–2013 AOD time series at IZO from ANNs

R. D. García et al.

Title Page

Abstract

Introduction

Conclusions

References

Tables

Figures



Back

Close

Full Screen / Esc

Printer-friendly Version

Interactive Discussion



1941–2013 AOD time series at IZO from ANNs

R. D. García et al.

Title Page

Abstract

Introduction

Conclusions

References

Tables

Figures



Back

Close

Full Screen / Esc

Printer-friendly Version

Interactive Discussion



values, with Pearson coefficients of 0.97 (AERONET/ANN) and 0.93 (Mark-I/ANN). At the longest time scale (1941–2009), we found a good agreement between ANN AOD monthly medians and the percentage of time the wind blows from the Sahara desert (SE) ($R = 0.86$), and also a good correlation between the number of days with AOD ≥ 0.20 and the number of days in which synoptical observations reported mineral dust events ($R = 0.89$). These results show the reliability of the reconstructed ANN AOD series, confirming its consistency in this long period (1941–2009), and capability for tracking inter-annual variations of dust-laden Saharan air mass outbreaks.

Finally, this paper also highlights the potential of ANNs to estimate AOD values and probe its suitability for long-term AOD series reconstruction. Thereby, the ANN methodology developed here for AOD series reconstruction might be suitable to be applied in Synoptic stations of North Africa, the Middle East and Asia, in which the reduced visibility is primarily due to the presence of mineral dust, and where recent AOD observations are available for validation.

Acknowledgements. This work was developed under the Specific Agreement of Collaboration between the Meteorological State Agency (AEMET) of Spain and the University of Valladolid regarding radiometry, ozone and atmospheric aerosol programmes conducted at Izaña Atmospheric Observatory (IZO), and for the adaptation and integration of the AEMET CIMEL network following the AERONET-RIMA standards. This study is also part of the activities carried out within the WMO CIMO Testbed for Aerosols and Water Vapor Remote Sensing instruments at Izaña Observatory. The AERONET Cimel sunphotometer at Izaña has been calibrated by AERONET-EUROPE Calibration Service, financed by the Aerosol Cloud and TRace gas InfraStructure (ACTRIS) European Research Infrastructure Action (FP7/2007-2013 No. 262254). Financial supports from the Spanish Ministry of Economy and Competitiveness (MINECO) and from the “Fondo Europeo de Desarrollo Regional” (FEDER) for project CGL2012-33576 is gratefully acknowledged. We thank the AERONET-GSFC, PHOTONS-LOA, RIMA-UVa, and RIMA-CIAI (AEMET) staff for their scientific and technical support. The authors are grateful to the IZO team and especially all observers who have worked in the past at Izaña Atmospheric Observatory. We also acknowledge our colleague Celia Milford for improving the English language of the manuscript.

References

- Angström, A. K.: On the atmospheric transmission of sun radiation and on the dust in the air, *Geogr. Ann.*, 12, 130–159, 1929. 9085
- Barreto, A., Cuevas, E., Pallé, P., Romero, P. M., Guirado, C., Wehrli, C. J., and Almansa, F.: Recovering long-term aerosol optical depth series (1976–2012) from an astronomical potassium-based resonance scattering spectrometer, *Atmos. Meas. Tech.*, 7, 4103–4116, doi:10.5194/amt-7-4103-2014, 2014. 9077, 9080, 9084, 9085
- Cazorla, A., Olmo, F. J., and Alados-Arboledas, L.: Using a sky imager for aerosol characterization, *Atmos. Environ.*, 42, 2739–2745, 2008. 9078
- Cerdeña, A., González, A., and Pérez, J. C.: Remote sensing of water cloud parameters using neural networks, *J. Atmos. Ocean. Tech.*, 24, 52–63, doi:10.1175/JTECH1943.1, 2006. 9078
- Cuevas, E.: Estudio del Comportamiento del Ozono Troposférico en el Observatorio de Izaña (Tenerife) y su Relación con la Dinámica Atmosférica, Thesis, Univ. Complutense de Madrid at Spain, available at: <http://www.ucm.es/BUCM/tesis/19911996/X/1/X1023101.pdf>, 1996 (in Spanish). 9080
- Cuevas, E., González, Y., Rodríguez, S., Guerra, J. C., Gómez-Peláez, A. J., Alonso-Pérez, S., Bustos, J., and Milford, C.: Assessment of atmospheric processes driving ozone variations in the subtropical North Atlantic free troposphere, *Atmos. Chem. Phys.*, 13, 1973–1998, doi:10.5194/acp-13-1973-2013, 2013. 9080
- Cuevas, E., Milford, C., Bustos, J. J., del Campo-Hernández, R., García, O. E., García, R. D., Gómez-Peláez, A. J., Ramos, R., Redondas, A., Reyes, E., Rodríguez, S., Romero-Campos, P. M., Schneider, M., Belmonte, J., Gil-Ojeda, M., Almansa, F., Alonso-Pérez, S., Barreto, A., Guirado-Fuentes, C., López-Solano, C., Afonso, S., Bayo, C., Berjón, A., Bethencourt, J., Camino, C., Carreño, V., Castro, N. J., Cruz, A. M., Damas, M., De Ory-Ajamil, F., García, M. I., Fernández-de Mesa, C. M., González, Y., Hernández, C., Hernández, Y., Hernández, M. A., Hernández, B., Jover, M., Kühn, S. O., López-Fernández, R., López-Solano, J., Peris, A., Rodríguez-Franco, J. J., Sálamó, C., Sepúlveda, E., and Sierra-Ramos, M.: Izaña Atmospheric Research Center Activity Report 2012–2014, edited by: Cuevas, E. and Milford, C., NIPO: 281-15-004-2, State Meteorological Agency (AEMET), Madrid, Spain, 2015a. 9080
- Cuevas, E., Camino, C., Benedetti, A., Basart, S., Terradellas, E., Baldasano, J. M., Morcrette, J. J., Marticorena, B., Goloub, P., Mortier, A., Berjón, A., Hernández, Y., Gil-Ojeda, M.,

AMTD

8, 9075–9103, 2015

1941–2013 AOD time series at IZO from ANNs

R. D. García et al.

Title Page

Abstract

Introduction

Conclusions

References

Tables

Figures



Back

Close

Full Screen / Esc

Printer-friendly Version

Interactive Discussion



1941–2013 AOD time series at IZO from ANNs

R. D. García et al.

Title Page

Abstract

Introduction

Conclusions

References

Tables

Figures



Back

Close

Full Screen / Esc

Printer-friendly Version

Interactive Discussion



and Schulz, M.: The MACC-II 2007–2008 reanalysis: atmospheric dust evaluation and characterization over northern Africa and the Middle East, *Atmos. Chem. Phys.*, 15, 3991–4024, doi:10.5194/acp-15-3991-2015, 2015b. 9080

De Bruin, H. A. R., Van den Hurk, B. J. J. M., and Welgraven, D.: A series of global radiation at Wageningen for 1928–1992, *Int. J. Climatol.*, 15, 1253–1272, doi:10.1002/joc.3370151106, 1995. 9077

Dirección General del Instituto Geográfico y Estadístico: Observatorio Atmosférico de Izaña, Anual del Observatorio Central Meteorológico, Suplemento al tomo III, Madrid, 1915. 9079

Demuth, H. and Beale, M.: Neural network toolbox for use with MATLAB, USA, The MathWorks Inc, 1993. 9081

Dorvlo, A. S., Jervase, J. A., and Al-Lawati, A.: Solar radiation estimation using artificial neural networks, *Appl. Energ.*, 71, 307–319, 2002. 9078

Eck, T. F., Holben, B. N., Reid, J. S., Dubovik, O., Smirnov, A., O'Neill, N. T., Slutsker, I., and Kinne, S.: Wavelength dependence of the optical depth of biomass burning, urban, and desert dust aerosols, *J. Geophys. Res.*, 104, 31333–31349, doi:10.1029/1999JD900923, 1999. 9085

Feister, U. and Junk, J.: Reconstruction of daily solar UV irradiation by an Artificial Neural Network, *SPIE*, 63622H, 6362–94, 1–11, 2006. 9078

Feister, U., Junk, J., Woldt, M., Bais, A., Helbig, A., Janouch, M., Josefsson, W., Kazantzidis, A., Lindfors, A., den Outer, P. N., and Slaper, H.: Long-term solar UV radiation reconstructed by ANN modelling with emphasis on spatial characteristics of input data, *Atmos. Chem. Phys.*, 8, 3107–3118, doi:10.5194/acp-8-3107-2008, 2008. 9078

Foresee, F. D. and Hagan, M. T.: Gauss-Newton approximation to Bayesian learning, in: Proceedings of the 1997 international joint conference on neural networks, Vol. 3, IEEE, Piscataway, 1930–1935, 1997. 9082

Foyo-Moreno, I., Alados, I., Antón, M., Fernández-Gálvez, J., Cazorla, A., and Alados-Arboledas, L.: Estimating aerosol characteristics from solar irradiance measurements at an urban location in southeastern Spain, *J. Geophys. Res.-Atmos.*, 119, 1845–1859, 2014. 9078

García, R. D., Cuevas, E., García, O. E., Cachorro, V. E., Pallé, P., Bustos, J. J., Romero-Campos, P. M., and de Frutos, A. M.: Reconstruction of global solar radiation time series from 1933 to 2013 at the Izaña Atmospheric Observatory, *Atmos. Meas. Tech.*, 7, 3139–3150, doi:10.5194/amt-7-3139-2014, 2014a. 9084

1941–2013 AOD time series at IZO from ANNs

R. D. García et al.

Title Page

Abstract

Introduction

Conclusions

References

Tables

Figures



Back

Close

Full Screen / Esc

Printer-friendly Version

Interactive Discussion



- García, R. D., García, O. E., Cuevas, E., Cachorro, V. E., Romero-Campos, P. M., Ramos, R., and de Frutos, A. M.: Solar radiation measurements compared to simulations at the BSRN Izaña station, Mineral dust radiative forcing and efficiency study, *J. Geophys. Res.*, 119, 179–194, doi:10.1002/2013JD020301, 2014b. 9076, 9077, 9083, 9084
- 5 Gilgen, H., Wild, M., and Ohmura, A.: Means and trends of shortwave irradiance at the surface estimated from GEBA, *J. Climate*, 11, 2042–2061, 1998. 9077
- González, A., Pérez, J. C., Herrera, F., Rosa, F., Wetzel, M. A., Borys, R. D., and Lowenthal, D. H.: Stratocumulus properties retrieval method from NOAA-AVHRR data based on the discretization of cloud parameters, *Int. J. Remote Sens.*, 23, 627–645, 2002. 9078
- 10 González, Y., Schneider, M., Rodríguez, S., Cuevas, E., Dyroff, C., Christner, E., Andrey, J., García, O., Sepúlveda, E.: Measurements and interpretation of the water vapor δD variability at Izaña North Atlantic free troposphere site, Symposium on Atmospheric Chemistry and Physics at Mountain Sites, Steamboat Springs, CO, USA, 11–15 August 2014, available at: <http://izana.aemet.es> (last access: 1 September 2015), 2014. 9098
- 15 Hao, Y. and Wilamowski, B. M.: Levenberg–Marquardt Training. *Industrial Electronics Handbook*, vol. 5, Intelligent Systems, 2nd edn., chapter 12, 12-1–12-15, CRC Press, Boca Raton, 2011. 9082
- Holben, B. N., Tanré, D., Smirnov, A., Eck, T. F., Slutsker, I., Abuhassan, N., Newcomb, W. W., Schafer, J. S., Chatenet, B., Lavenu, F., Kaufman, Y. J., Vande Castle, J., Setzer, A., Markham, B., Clark, D., Frouin, R., Halthore, R., Karneli, A., O'Neill, N. T., Pietras, C., Pinker, C., Voss, K., and Zibordi, G.: An emerging ground-based aerosol climatology: Aerosol Optical Depth from AERONET, *J. Geophys. Res.-Atmos.*, 106, 12067–12097, doi:10.1029/2001JD900014, 2001. 9077
- 20 Jain, A. K., Mao, J., and Mohiuddin, K. M.: Artificial neural networks: a tutorial, *Computer*, 3, 31–44, 1996. 9081
- Junk, J., Feister, U., and Helbig, A.: Reconstruction of daily solar UV irradiation from 1893 to 2002 in Potsdam, Germany, *Int. J. Biometeorol.*, 51, 505–512, 2007. 9078
- Kaufman, Y. J., Gitelson, A., Karnieli, A., Ganor, E., and Fraser, R. S.: Size distribution and phase function of aerosol particles retrieved from sky brightness measurements, *J. Geophys. Res.-Atmos.*, 99, 10331–10356, 1994. 9080
- 30 Kaufman, Y. J., Tanré, D., and Boucher, O.: A satellite view of aerosols in the climate system, *Nature*, 419, 215–223, 2002. 9077

1941–2013 AOD time series at IZO from ANNs

R. D. García et al.

Title Page

Abstract

Introduction

Conclusions

References

Tables

Figures



Back

Close

Full Screen / Esc

Printer-friendly Version

Interactive Discussion



- Kim, D., Chin, M., Yu, H., Eck, T. F., Sinyuk, A., Smirnov, A., and Holben, B. N.: Dust optical properties over North Africa and Arabian Peninsula derived from the AERONET dataset, *Atmos. Chem. Phys.*, 11, 10733–10741, doi:10.5194/acp-11-10733-2011, 2011. 9080
- 5 Kudo, R., Uchiyama, A., Yamazaki, A., Sakami, T., and Iijima, O.: Decadal changes in aerosol optical thickness and single scattering albedo estimated from ground-based broadband radiometers: a case study in Japan, *J. Geophys. Res.-Atmos.*, 116, D03207, doi:10.1029/2010JD014911, 2011. 9077
- Lanzante, J. R.: Resistant, robust and nonparametric techniques for the analysis of climate data: Theory and examples including applications to historical radiosonde station data, *Int. J. Climatol.*, 16, 1197–1226, 1996. 9086
- 10 Linares-Rodríguez, A., Ruiz-Arias, J. A., Pozo-Vázquez, D., and Tovar-Pescador, J.: Generation of synthetic daily global solar radiation data based on ERA-Interim reanalysis and artificial neural networks, *Energy*, 36, 5356–5365, 2011. 9078
- Linares-Rodríguez, A., Ruiz-Arias, J. A., Pozo-Vázquez, D., and Tovar-Pescador, J.: An artificial neural network ensemble model for estimating global solar radiation from Meteosat satellite images, *Energy*, 61, 636–645, 2013. 9078
- 15 López, G., Batlles, F. J., and Tovar-Pescador, J.: Selection of input parameters to model direct solar irradiance by using artificial neural networks, *Energy*, 30, 1675–1684, 2005. 9078
- Mohandes, M., Rehman, S., and Halawani, T. O.: Estimation of global solar radiation using artificial neural networks, *Renew. Energ.*, 14, 179–184, doi:10.1016/S0960-1481(98)00065-2, 1998. 9078
- 20 Ohmura, A.: Observed long-term variations of solar irradiances at the Earth's surface, *Space Sci. Rev.*, 125, 111–128, 2006. 9077
- Ohmura, A. and Lang, H.: Secular variation of global radiation over Europe, in: *Current Problems in Atmospheric Radiation*, edited by: Lenoble, J. and Geleyn, J. F., A. Deepak, Hampton, Va, 298–301, 1989. 9077
- 25 Ohvril, H., Teral, H., Neiman, L., Kannel, M., Uustare, M., Tee, M., Russak, V., Okulov, O., Joveer, A., Kallis, A., Ohvril, T., Terez, E. I., Terez, G. A., Gushchin, G. K., Abakumova, G. M., Gorbarenko, E. V., Tsvetkov, A. V., and Laulainen, N.: Global dimming and brightening versus atmospheric column transparency, Europe, 1906–2007, *J. Geophys. Res.-Atmos.*, 114, D00D12, doi:10.1029/2008JD010644, 2009. 9077
- 30

1941–2013 AOD time series at IZO from ANNs

R. D. García et al.

Title Page

Abstract

Introduction

Conclusions

References

Tables

Figures



Back

Close

Full Screen / Esc

Printer-friendly Version

Interactive Discussion



- Paoli, C., Voyant, C., Muselli, M., and Nivet, M. L.: Solar radiation forecasting using ad-hoc time series preprocessing and neural networks, in: *Emerging Intelligent Computing Technology and Applications*, Springer, Berlin Heidelberg, 898–907, 2009. 9078
- Pallé, E. and Butler, C. J.: Sunshine records from Ireland: Cloud factors and possible links to solar activity and cosmic rays, *Int. J. Climatol.*, 21, 709–729, doi:10.1002/joc.657, 2001. 9076
- Prospero, J., Ginoux, P., Torres, O., and Nicholson, S.: Environmental characterization of global sources of atmospheric soil dust derived from the NIMBUS7 (TOMS) absorbing aerosol product, *Review Geophys.*, 40, 1002, doi:10.1029/2000RG000095, 2002. 9080
- Retalis, A., Hadjimitsis, D. G., Michaelides, S., Tymvios, F., Chrysoulakis, N., Clayton, C. R. I., and Themistocleous, K.: Comparison of aerosol optical thickness with in situ visibility data over Cyprus, *Nat. Hazards Earth Syst. Sci.*, 10, 421–428, doi:10.5194/nhess-10-421-2010, 2010. 9082
- Rodríguez, S., Alastuey, A., Alonso-Pérez, S., Querol, X., Cuevas, E., Abreu-Afonso, J., Viana, M., Pérez, N., Pandolfi, M., and de la Rosa, J.: Transport of desert dust mixed with North African industrial pollutants in the subtropical Saharan Air Layer, *Atmos. Chem. Phys.*, 11, 6663–6685, doi:10.5194/acp-11-6663-2011, 2011. 9080
- Rodríguez, S., Cuevas, E., Prospero, J. M., Alastuey, A., Querol, X., López-Solano, J., García, M. I., and Alonso-Pérez, S.: Modulation of Saharan dust export by the North African dipole, *Atmos. Chem. Phys.*, 15, 7471–7486, doi:10.5194/acp-15-7471-2015, 2015. 9080
- Sanchez-Lorenzo, A., Brunetti, M., Calbo, J., and Martin-Vide, J.: Recent spatial and temporal variability and trends of sunshine duration over the Iberian Peninsula from a homogenized data set, *J. Geophys. Res.*, 112, D20115, doi:10.1029/2007JD008677, 2007. 9076, 9077
- Shaw, G. E.: Aerosols at Mauna Loa, optical properties, *J. Atmos. Sci.*, 36, 862–869, 1979. 9077
- Stanhill, G. and Cohen, S.: Global dimming: a review of the evidence for a widespread and significant reduction in global radiation, *Agr. Forest Meteorol.*, 107, 255–278, doi:10.1016/S0168-1923(00)00241-0, 2001. 9076, 9077
- Thies, C.: *Instruction Manual Hygro-thermo transmitter compact*, Adolf THIES GmbH & Co. KG, Göttingen, Alemania, 2011. 9084
- Wehrli, C.: Calibrations of filter radiometers for determination of atmospheric optical depth, *Metrologia*, 37, 419–422, 2000. 9082
- Wild, M.: Global dimming and brightening: a review, *J. Geophys. Res.*, 114, D00D16, doi:10.1029/2008JD011470, 2009. 9076, 9077

1941–2013 AOD time series at IZO from ANNs

R. D. García et al.

Title Page

Abstract

Introduction

Conclusions

References

Tables

Figures



Back

Close

Full Screen / Esc

Printer-friendly Version

Interactive Discussion



- Wild, M., Gilgen, H., Roesch, A., Ohmura, A., Long, C. N., Dutton, E. G., Forgan, B., Kallis, A., Russak, V., and Tsvetkov, A.: From dimming to brightening: decadal changes in surface solar radiation, *Science*, 308, 847–850, doi:10.1126/science.1103215, 2005. 9077
- 5 Wild, M., Grieser, J., and Schär, C.: Combined surface solar brightening and increasing greenhouse effect support recent intensification of the global land-based hydrological cycle, *Geophys. Res. Lett.*, 35, L17706, doi:10.1029/2008GL034842, 2008. 9077
- World Meteorological Organization (WMO): Guide to meteorological instruments and methods of observation, 6th edn., WMO no. 8. Secretariat of the World Meteorol. Organ., Geneva, Switzerland, 1996. 9082
- 10 World Meteorological Organization (WMO): Manual on Codes, Regional Codes and National Coding Practices, Volume II, Secretariat of the World Meteorological Organization, Geneva, Switzerland, WMO 306, 1998. 9086

1941–2013 AOD time series at IZO from ANNs

R. D. García et al.

Table 2. Statistics of the difference between non-perturbed and perturbed ANN AOD estimates ($AOD - (AOD \pm \delta)$): Pearson correlation coefficient (R) between the differences and ANN AOD values, standard deviation (SD) and median of the difference time series (systematic bias). “All” represents the error estimation considering the uncertainties of all parameters together ($VIS \pm 25\%$, $FCS \pm 5$ and $RH \pm 2\%$).

AOD Ranges	Input	R	SD	Systematic Bias
≤ 0.10 (102 days)	RH	0.08	0.02	-0.01
	FCS	0.06	0.09	-0.01
	VIS	0.05	0.04	-0.01
	All	0.01	0.12	-0.02
≥ 0.20 (15 days)	RH	-0.26	0.05	0.01
	FCS	0.03	0.16	-0.04
	VIS	-0.21	0.07	0.01
	All	-0.01	0.17	0.03
All AOD range	–	0.16	0.13	0.03

[Title Page](#)
[Abstract](#)
[Introduction](#)
[Conclusions](#)
[References](#)
[Tables](#)
[Figures](#)
[◀](#)
[▶](#)
[◀](#)
[▶](#)
[Back](#)
[Close](#)
[Full Screen / Esc](#)
[Printer-friendly Version](#)
[Interactive Discussion](#)


1941–2013 AOD time series at IZO from ANNs

R. D. García et al.

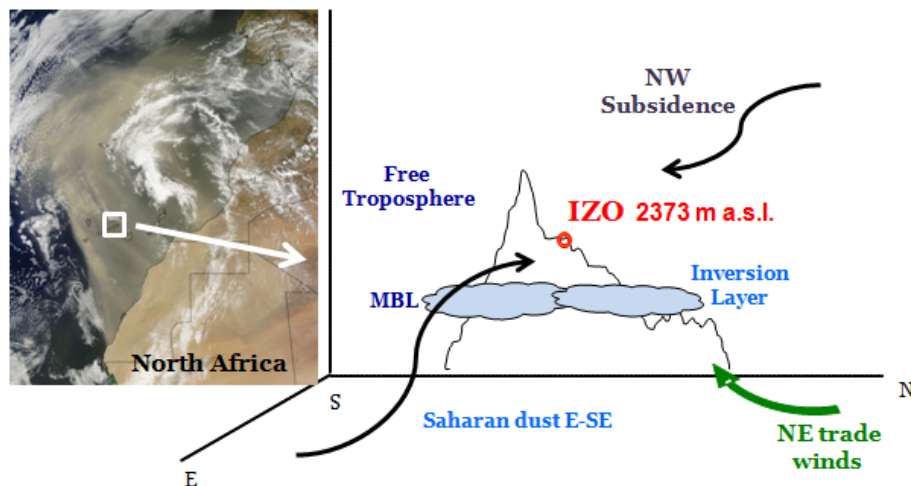


Figure 1. (a) MODIS/Terra image showing a strong Saharan dust outbreak over the study area (the Canary Islands) on 25 June 2012; (b) vertical cross-section of Tenerife Island with a scheme of the vertical atmospheric stratification (Marine Boundary Layer (MBL), Inversion Layer, and Free Troposphere) and the main atmospheric flows affecting IZO (NW clean subtropical subsident air masses, low level NE trade winds, and E–SE Saharan dust intrusions). This figure has been adapted from González et al. (2014).

Title Page

Abstract

Introduction

Conclusions

References

Tables

Figures

◀

▶

◀

▶

Back

Close

Full Screen / Esc

Printer-friendly Version

Interactive Discussion



1941–2013 AOD time series at IZO from ANNs

R. D. García et al.

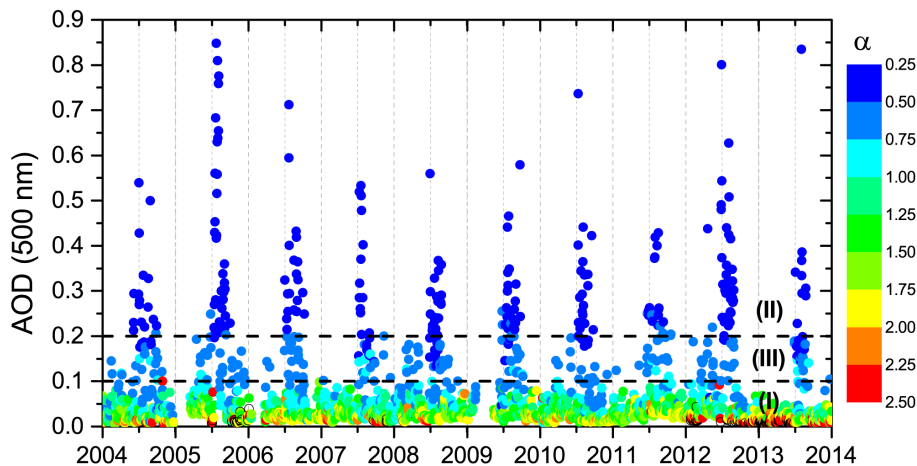
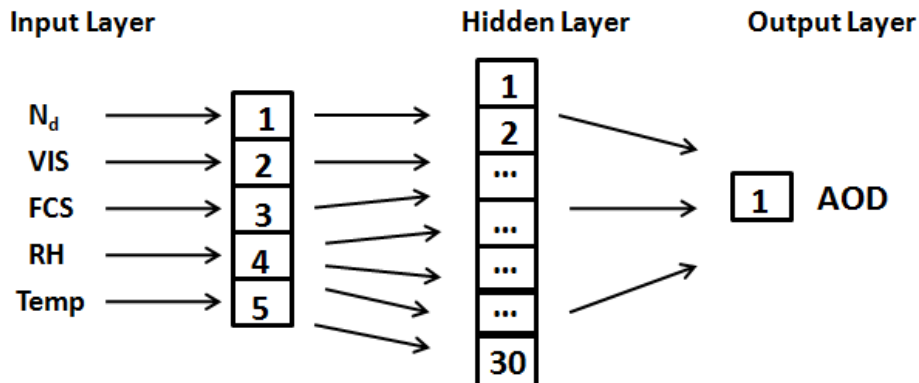


Figure 2. Daily AOD at 500 nm time series from AERONET between 2004 and 2013 at IZO. The color scale indicates the daily Angström Exponent (α) values. The dashed lines distinguish the different AOD- α zones: (I) $\text{AOD} \leq 0.10$ and $\alpha \geq 0.75$; (II) $\text{AOD} \geq 0.20$ and $\alpha \leq 0.50$, and (III) $0.10 < \text{AOD} < 0.20$ and $0.50 < \alpha < 0.75$.

[Title Page](#)[Abstract](#)[Introduction](#)[Conclusions](#)[References](#)[Tables](#)[Figures](#)[Back](#)[Close](#)[Full Screen / Esc](#)[Printer-friendly Version](#)[Interactive Discussion](#)

1941–2013 AOD time series at IZO from ANNs

R. D. García et al.

**Figure 3.** Schematic representation of the artificial neural network used in this study.[Title Page](#)[Abstract](#)[Introduction](#)[Conclusions](#)[References](#)[Tables](#)[Figures](#)[◀](#)[▶](#)[◀](#)[▶](#)[Back](#)[Close](#)[Full Screen / Esc](#)[Printer-friendly Version](#)[Interactive Discussion](#)

1941–2013 AOD time series at IZO from ANNs

R. D. García et al.

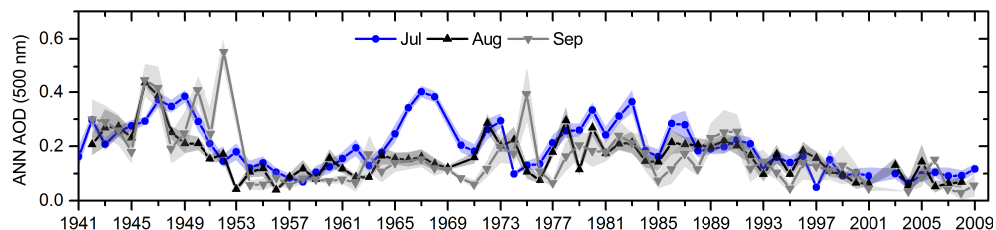


Figure 4. Times series of the ANN AOD monthly medians (July, August and September) at 500 nm between 1941 and 2009 at IZO. Shadings show the range of ± 1 SEM (standard error of the monthly median).

[Title Page](#)[Abstract](#)[Introduction](#)[Conclusions](#)[References](#)[Tables](#)[Figures](#)[Back](#)[Close](#)[Full Screen / Esc](#)[Printer-friendly Version](#)[Interactive Discussion](#)

1941–2013 AOD time series at IZO from ANNs

R. D. García et al.

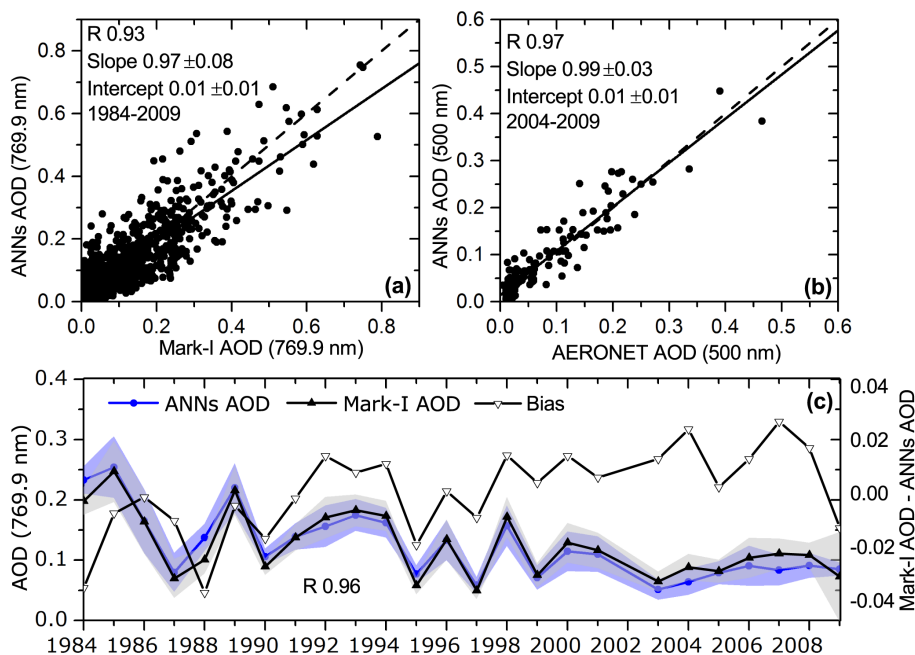


Figure 5. Scatterplot of ANN AOD estimates vs. **(a)** daily Mark-I AOD at 769.9 nm for all the cloud-free days (oktas = 0) and **(b)** daily AERONET AOD at 500 nm for the periods 1984–2009 and 2004–2009, respectively. The black solid lines are the least-square fits and the dotted lines are the diagonals. The least-square fit parameters are shown in the legend (Pearson correlation coefficient, R , slope and intercept). **(c)** Time series of monthly medians of Mark-I AOD and ANN AOD estimates in July (on the left axis) and time series of the differences between these AOD values (on the right axis). Shadings show the range of ± 1 SEM (standard error of the monthly median).

1941–2013 AOD time series at IZO from ANNs

R. D. García et al.

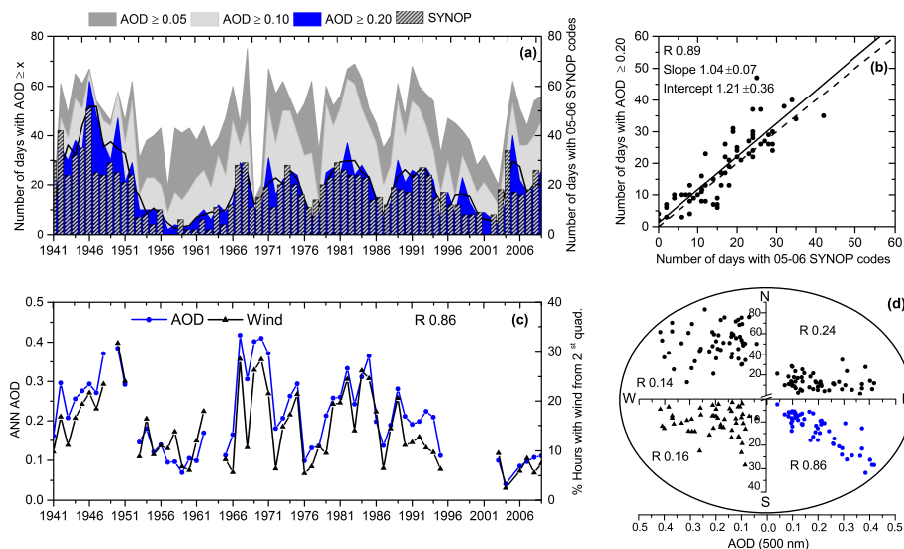


Figure 6. (a) Time series of the number of days grouped into ANN AOD intervals ($AOD \geq 0.05$; $AOD \geq 0.10$; $AOD \geq 0.20$) on the left axis, while on the right axis, the bars indicate the number of days with SYNOP data reporting dust in suspension (05-06 SYNOP codes) for the period 1941–2009. The five-yr running mean is shown in black. (b) Scatterplot of number of days with ANN AOD ≥ 0.20 and number of days with 05-06 SYNOP codes. The least-square fit parameters are shown in the legend. (c) Time series of the ANN AOD monthly medians (blue line) and monthly percentage of time the wind blows from the second quadrant (E–S; 90 – 180°) (black line) at IZO in July in the period 1941–2009. (d) Percentage of time (y axis) the wind blows from in each one of the four quadrants vs. the ANN AOD monthly medians (x axis). R indicates the Pearson coefficient.